Evaluation of Hemodynamic Response Function in Vision and Motor Brain Regions for the Young and Elderly Adults

Hassan Morsheddost [1], Davud Asemani [1]*, Mahsa Alizadeh Shalchy [1]

1. Department of Biomedical Engineering, Faculty of Electrical Engineering, K. N. Toosi University of Technology, Tehran, Iran.

Article info:
Received: 05 April 2014
First Revision: 22 June 2014
Accepted: 11 November 2014

Key Words:
Aging, Hemodynamic Response Function, fMRI, Denoising, MDL

ABSTRACT

Introduction: Prior studies comparing Hemodynamic Response Function (HRF) in the young and elderly adults based on fMRI data have reported inconsistent findings for brain vision and motor regions in healthy aging. It is shown that the averaging method employed in all previous works has caused this inconsistency. The averaging is so sensitive to outliers and noise. However, fMRI data are obscured with a major contribution of noise particularly in the elderly case.

Methods: Deconvolution algorithm is here proposed for HRF extraction to achieve more robustness against noise. In spite of earlier works, proposed deconvolution algorithm yields compatible HRF results using either original or denoised fMRI data, though a large percentage of selected active voxels change in the latter case. In the current study, event-related fMRI data have been used for 18 subjects (8 young and 10 elderly adults) with a simple visual and motor task of pressing a key with index in response to the visual presentation of the word tap. Considering anatomically-defined vision and motor regions and preprocessing steps in FSL and SPM, the activated voxels have been selected according to t-test for which HRF is estimated using deconvolution method.

Results: Experimental results demonstrate that HRF peak amplitudes do not differ significantly ($P=0.8$) in the vision region for the young and the elderly. In motor region, the HRF peak significantly increases for the young compared to the elderly ($P<0.03$). Repeating the procedure on the denoised fMRI data using MDL algorithm, the same results have been obtained.

Discussion: In this study, a comparative study has been realized on the hemodynamic response properties associated with the young and the elderly adults on a simple visual and motor task.

1. Introduction

Medical imaging is a fundamental area in modern medicine. Of the several MRI modalities, functional MRI (fMRI) represents a promising and exciting method that, among other purposes, may determine the involvement of brain regions regarding a particular task. The task includes any brief sensory or cognitive stimulation such as sounds, visual images and gentle touching of the skin.

Although MRI have been around since the 1980s for anatomical clinical purposes (e.g. for brain tumor stroke and multiple sclerosis analysis), it was only in 1990 when Ogawa showed that the MRI water signals can be sensitized to cerebral oxygenation, using deoxyhemoglobin as an endogenous susceptibility contrast agent. Using gradient-echo imaging sensitivity to the local inhomogeneity of the static magnetic field, Ogawa demonstrated (in an animal model) that the appearance of the brain blood vessels changed with blood oxygenation. Within two years, his group and two others had published papers using this Blood-Oxygenation-Level-Dependent (BOLD) contrast MRI to detect brain activa-

* Corresponding Author:
Davud Asemani, PhD
Address: Department of Biomedical Engineering, Faculty of Electrical Engineering, K. N. Toosi University of Technology, Tehran, Iran.
Tel.: +98 (21) 8406-2405
Fax:+98 (21) 8846-2066
E-mail: Asemani@eetd.kntu.ac.ir

tion in humans (Ogawa et al., 1993; Ogawa et al., 1992; Bandettini, Wong, Hinks, Tikofsky, & Hyde, 1992), and today, an explosion of studies is based on this so-called fMRI technique to map human brain function.

During functional magnetic resonance imaging, a brief focal neural activation evokes what is called a Hemodynamic time-course Response Function (HRF) associated with age (Powers, 2000: 33-80) and that a BOLD time series data is modeled as the convolution between this invariant HRF and an impulse train of neural events (Boynton, Engel, Glover, & Heeger, 1996). However, how aging affects the fMRI signal has not been totally identified.

Several prior studies comparing hemodynamic response properties in the young and elderly adults using fMRI have led to partially-opposite results (Gauthier et al., 2013; Mohtasib et al., 2012; Aizenstein et al., 2004; Huettel, Singerman, & McCarthy, 2001; Buckner, Snyder, Sanders, Raichle, & Morris, 2000; D'Esposito, Zarahn, Aguirre, & Rypma, 1999; Ross et al., 1997) (summarized in Table 2). Aizenstein et al., (2004) investigated hemodynamic responses in young and elderly adults using an event related sensory–motor paradigm. In their study, the HRF has been simply extracted by averaging procedure. They found the same HRF peak amplitudes for both the young and the elderly in either vision or motor Region-Of-Interests (ROIs). Huettel et al.m (2001) and D'Esposito et al., (1999) reported similar HRF amplitude peaks using averaging method as well, though showed also an evident decrease of Signal-to-Noise Ratio (SNR) in the elderly case.

In contrast to these results, Mohtasib et al., (2012) reported, though Cerebral Blood Flow (CBF) response remains the same, but the BOLD response significantly intensifies for the aged adults compared to the young. Then, the increase of BOLD peak with aging was interpreted to associate with a significant reduction in either the oxygen metabolism response or the neural activity. The largest BOLD increase was reported to occur in the left and right medial frontal gyrus and the primary motor cortex. Using an event related sensory–motor paradigm and averaging scheme, Buckner et al., (2000) compared HRFs for the young and non-demented elderly adults as well. According to this study, HRF amplitude peaks appear to be different between the young and the elderly in vision ROI.

The motor ROI was nevertheless reported to exhibit the similar amplitude peaks but with a subtle time shift between the young and the elderly. Considering a block design paradigm, Ross et al., (1997) reported a significant decrease in the HRF of the elderly subjects compared to the young vision ROI. On the opposite, Gauthier et al., (2013) also found a decrease HRF peak in the elderly in comparison to the young, though neuronal activity and hemodynamic response were assumed to remain unchanged across the lifespan.

Trying to interpret the discrepancy of the results, Aizenstein et al., (2004) suppose the abnormality appears because of the negative deactivating voxels included in the HRF estimation and take the negative voxels out of their HRF estimation. They address the problem of the reduced activity, already reported for the elderly adults, to inclusion of these voxels. In this paper, the contradictory results are analyzed and it is shown that the inconsistent findings have been originated from the simple HRF estimation algorithm of averaging shared by all previous works.

Averaging method exhibits a large sensitivity to outliers particularly in fMRI data because of small number of scans at each Time of Repetition (TR) period. Moreover, averaging on individual HRF scanning periods renders the noise so critical especially in the elderly case. It is reminded that noise contribution is very dominant particularly for the elderly adults (D'Esposito, Deouell, & Gazzaley, 2003; Huettel et al., 2001; D'Esposito et al., 1999).

In fact, there is no absolute hypothesis in the literature in this regard that HRF peak exhibits an increase, a decrease or no significant change for the elderly. It is still a research challenge as there are contradictory findings in the literature. This work tries to deal with this challenge and to show some probable reasons for contradictory findings of earlier works. The proposed result should be justified through more clinical experimentations. More work is in progress on this challenge and justification procedure through applying the proposed method to other fMRI data bank to validate the results.

The current study exploits another method for extracting HRF. BOLD time-series data are here modeled as the convolution between an invariant HRF and an impulse train of neural events (Boynton, Engel, Glover, & Heeger, 1996) and the averaging is then replaced by deconvolution.

The selection of active voxels is here implemented by statistical t-test (positive t-value) as mentioned in Aizenstein et al., (2004). Also, to avoid the noise effects, Minimum Description Length (MDL) methods are uti-

lized for denosing based on powerful tools of wavelet (Mosheddost, Asemani, & Mirahadi, 2014; Roos, Myllymaki, & Rissanen, 2009; Bazargani, & Nosratinia, 2008; Rissanen, 2000). For experimental analysis, the fMRI data of 8 young and 10 elderly subjects participating in a simple finger-tapping fMRI study have been used in this paper like (Aizenstein et al., 2004).

2. Methods

2.1. Participants

Eighteen healthy right-handed subjects were analyzed in this study: 8 young healthy controls, 3 men, mean age =24.2 ± 4.37, and 10 healthy elderly subjects, 6 men, mean age=67.2 ± 4.83. Any subject with the following conditions has been excluded: alcoholism, depression, schizophrenia, bipolar affective disorder, prior history of stroke or significant head injury, Alzheimer's, Parkinson's, or Huntington's disease or taking psychotropic medications. The mean Mini-Mental State Exam score for the elderly subjects was 28.9 ± 0.99. Informed consent was obtained prior to scanning through procedures approved by the University of Pittsburgh Institutional Review Board. Each subject had been paid $75.

2.2. Stimuli

First, subjects were taught to perform a key-press with both index fingers every time they saw the word tap appearing on the screen. The stimulus appeared every 12 sec and remained on the screen for 1 sec. Subjects were instructed to fixate on a white cross-hair in the middle of the screen between the stimuli. There were 24 trials in a 5-min block. Stimulus presentation was performed by a Power Macintosh computer using the PsyScope software package (Cohen, MacWhinney, Flatt, & Provost, 1993). The stimuli were projected on a screen positioned above the subject's chest and the subject saw the screen through a series of mirrors. The stimuli subtended approximately 30^{o} of the visual field.

2.3. Image Acquisition

Imaging data were collected with a 1.5-T Signa scanner (GE Medical Systems), using one-shot spiral pulse sequence with TE=35 msec and T=2000 msec. High-resolution anatomical images (SPGRs) were acquired for each subject. For the functional data, 26 oblique axial slices were acquired with an in-plane resolution of 3.75 mm^2, a slice thickness of 3.8 mm, and a field of view of 240 mm^2.

2.4. fMRI Data preprocessing

The preprocessing stages are standard and the same as mentioned in Aizenstein et al., 2004. Also, the preprocessed fMRI data have been downloaded and used in this work from the data bank site. Motion correction was performed using MCFLIRT from the FSL package (Jenkinson, Bannister, Brady & Smith, 2002). To compensate the linear trend, a linear detrending algorithm was performed on data only within 3 SD of the mean same as Aizenstein et al., (2004). An outlier-correction algorithm was performed to remove data extending more than 7 SD from the mean. Global normalization was performed multiplicatively to give each subject a mean intensity of 3000. All analyses were conducted on each individual data after having transformed into standard MNI space. ROI selection of the vision and motor cortices was performed, where visual cortex is defined as the occipital cortex, the cuneus, and the precuneus, and motor cortex is defined as the precentral gyrus and the supplementary motor area. These regions are from the aal map obtained from the MRIcro software package (Tzourio-Mazoyer et al., 2002). These regions were then used to define motor and vision cortices in MNI single-subject's space.

To cross register each single subject data (anatomical and functional) onto standard MNI space, the following steps were performed. First, each subject's low-resolution mean functional image was registered to his/her high-resolution anatomical image. Then, each subject's high-resolution anatomical image was aligned with the MNI single-subject high-resolution anatomical image. Finally, both transform function in previous steps were concatenated in order to calculate a transform function which can register each subject's low-resolution func-

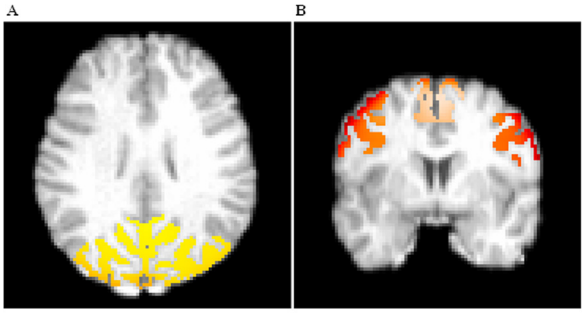

Figure 1. Automatic labeling of gray matter in (A) vision (occipital cortex, cuneus, and precuneus) and (B) motor (precentral gyrus and supplementary motor area) in a representative young subject. Selected vision region is shown in yellow; Selected motor region is colored red.

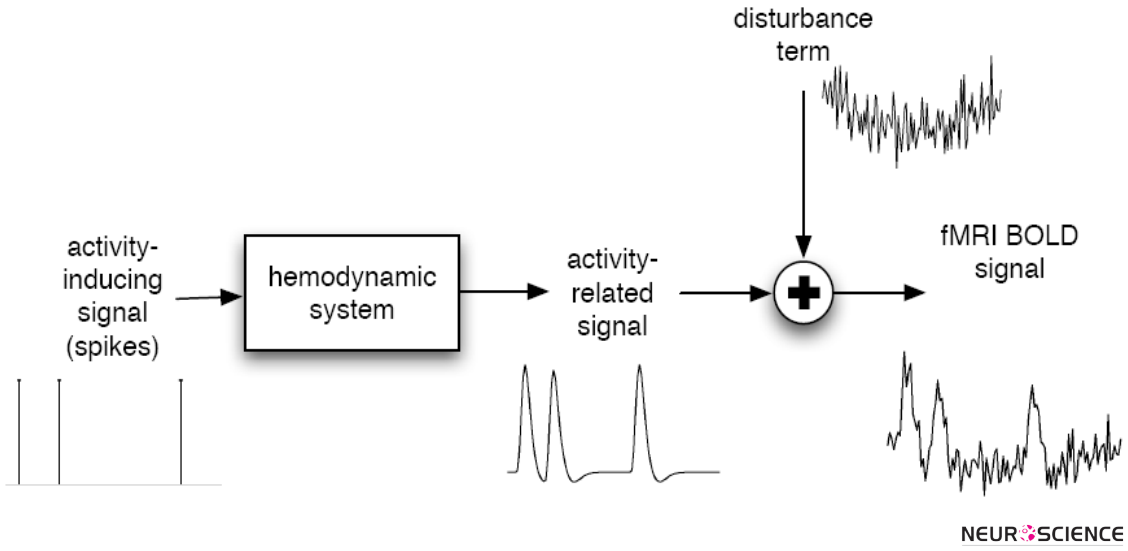

Figure 2. Hemodynamic system links neuronal activity to fMRI BOLD response, which is due to neurovascular coupling and a complex interplay between various physiological parameters.

tional images to the standard MNI space. The whole process was accomplished using the FLIRT algorithm in the FSL package with a 12-parameter affine option (Jenkinson, & Smith, 2001). Then, a gray matter mask was applied to each label using the FAST algorithm from the FSL package (Smith, 2002). The ROI selection of each subject was then visually inspected to assure an accurate ROI selection (see Figure 1 for a representative image).

2.5. fMRI Data analysis

2.5.1. Region-of-Interest Selection

First each subject's time series was constrained to the particular anatomic ROI (i.e. vision or motor) and then a t-test analysis has been performed on each subject's data, and contrasting the mean fMRI signal at the first scan in a trial with the signal at the third scan, that is, 4–6 sec after the finger tap when the HRF is expected to peak, to detect the activated voxels. To be consistent with earlier work Aizenstein et al., (2004) for comparison purposes, only 32 voxels have been used here as well with the highest t-values.

Also, the threshold value for thresholding t-values was independently chosen for each subject individual. The detection process has been applied to the fMRI time-series in two cases: original data and denoised data. Also, the results show that a considerable part of voxels (60 percent of these 32 voxels (Table 1)) change after applying denoising procedure.

2.5.2. HRF Extraction by Averaging

For each subject and for both ROIs, a time series was selected using only those voxels with a positive t-value. The HRF was generated by calculating the mean MR signal for each voxel at each of six time points (i.e. scans). Then, the mean of these HRFs was used as a final HRF. The resulting values were transformed into a percent change from baseline (time point 1) for standard presentation.

2.5.3 HRF Extraction by Deconvolution

BOLD time-series data are here modeled as the convolution between an invariant HRF and an impulse train of neural events (Boynton, Engel, Glover, & Heeger, 1996). For each subject and for both ROIs, a time series was selected using only those voxels with a positive t-value. The time series of selected voxel (BOLD signal) is imagined as the result of convolution between the respective HRF and stimulus impulses. Then, the HRF was deconvolved from BOLD time series by known stimulus train of impulses at the known onsets of the events (activity-inducing signal time) supposing a fixed length for HRF (see Figure 2 for time series creation). A linear regression approach is used to deconvolve the function.

Deconvlolution algorithm is here implemented in five steps as follows:

1. Consider matrix X initialized at zero of the size: time series × length of HRF.

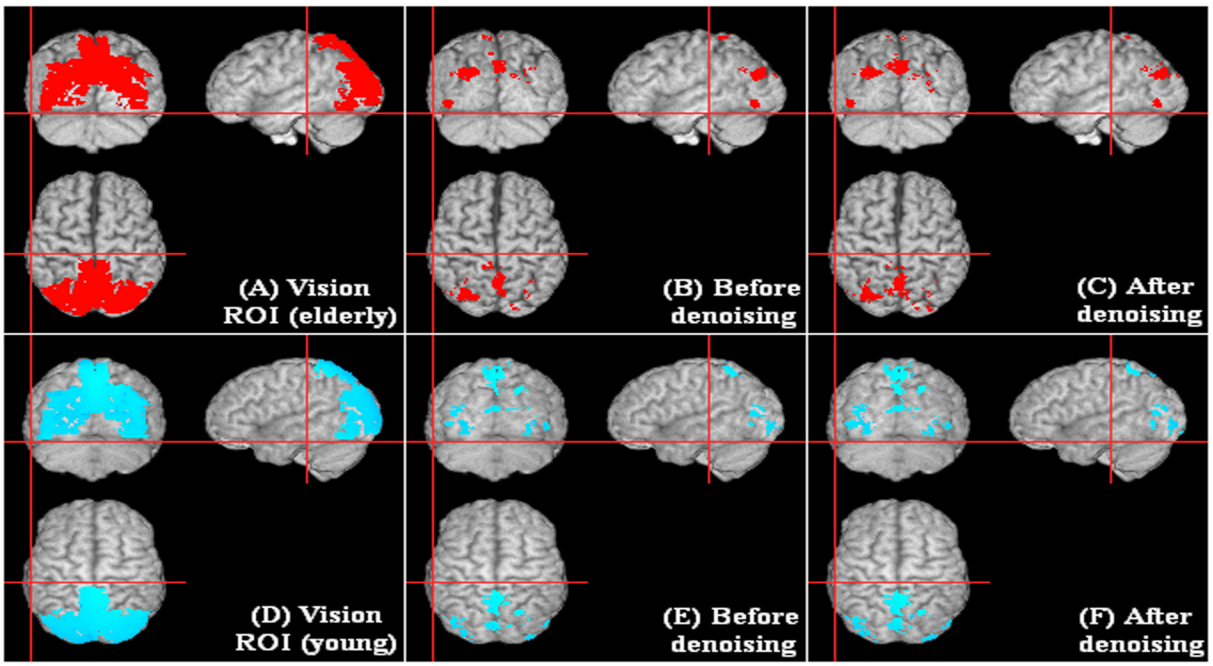

Figure 3. Automatic labeling of gray matter in visual cortex (occipital cortex, cuneus, and precuneus) for the elderly (A) and the young (D) subjects. Activation detection of fMRI data of visual cortex before (middle) and after (right) denosing by R-MDL. The elderly and the young subjects have been shown in top (A-C) and bottom (D-F) respectively.

2. Replace the diagonal elements with unity to associate with HRF elements.

3. Add a column of ones at 7th column of X. It is considered as a regressor to estimate the baseline.

4. Estimate the HRF by calculating Moore-Penrose pseudoinverse of matrix X and multiplying with time series.

5. HRF is corrected with adding the baseline.

2.5.4. Time series denoising

The time series of fMRI are often contaminated with noise which renders the data difficult for using informative parts in diagnosis. The noise contribution gets larger and more important through age increasing (D'Esposito, Deouell & Gazzaley, 2003; Huettel et al., 2001; & D'Esposito et al., 1999). The aim of denoising procedure is to remove any noise from an observed signal while keeping its desired informative part unchanged. Wavelet transform as a powerful tool has been widely used for denoising purposes (Mallat, 1998; Donoho & Johnstone, 1994). The threshold value plays an important role in the performance of denoising based on Discrete Wavelet Transform (DWT) (Donoho & Johnstone, 1994). There are many different methods for selecting the desired threshold such as VisuShrink (Donoho & Johnstone, 1994), SureShrink (Donoho & Johnstone, 1995), Minimum Description Length (MDL) or Crude MDL (C-MDL) (Rissanen, 2000) and Refined MDL (R-MDL) (Roos, Myllymaki, & Rissanen, 2009). R-MDL has been here used as optimized for fMRI data (Morsheddost et al., 2014).

In MDL method, the complexity of thresholding model (or the number of retained DWT coefficients) is determined automatically. In this study, the focus of the denoising is devoted to fMRI applications in which Hemodynamic Response Function (HRF) or activated voxels are looked for (Morsheddost et al., 2014; Bazargani, & Nosratinia 2008).

2.5.5. The Refined MDL Alghorithms

The observed time series, $y^n = (y^1,...,y^n)^T$, is supposed to be corrupted by additive noise (Consider the general linear model (GLM) at voxel), as following:

$$y^n = x^n + \varepsilon^n \quad (1)$$

Where the noise term ε^n is often assumed to be Gaussian and x^n is the desired noiseless time series (e.g. the Blood Oxygenation Level Dependent (BOLD) response). In fact, then the objective is to extract optimally

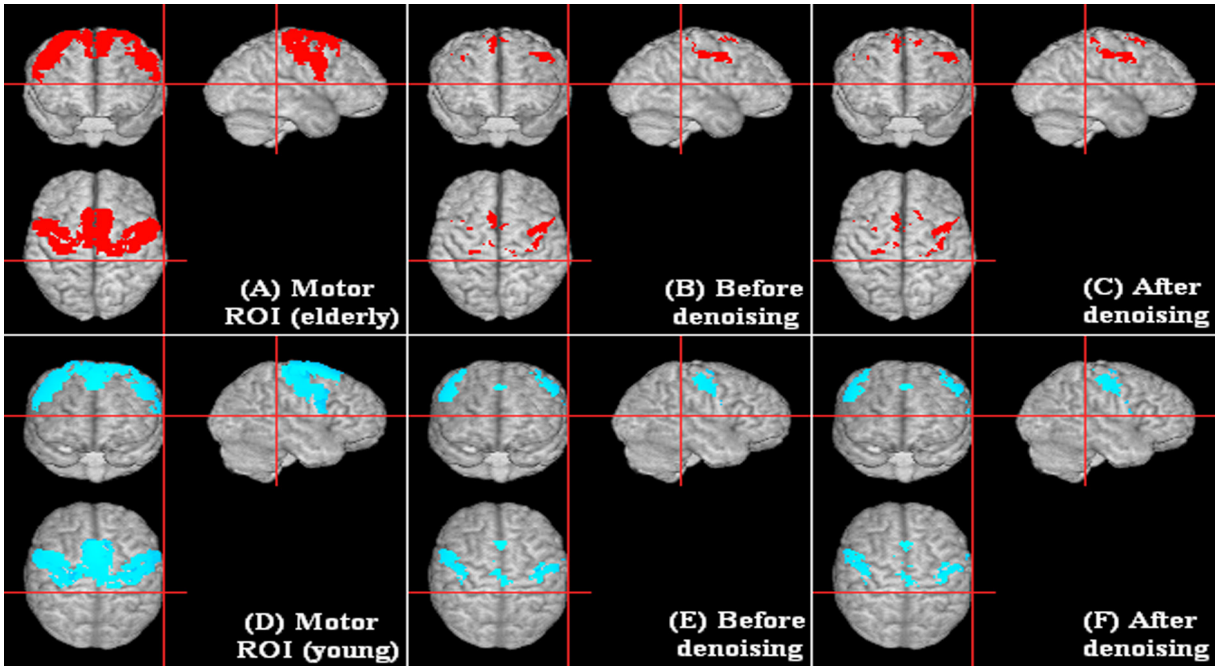

Figure 4. Automatic labeling of gray matter in motor cortex (occipital cortex, cuneus, and precuneus) for the elderly (A) and the young (D) subjects. Activation detection of fMRI data of motor cortex before (middle) and after (right) denosing by R-MDL. The elderly and the young subjects have been shown in top (A-C) and bottom (D-F) respectively.

the uncorrupted original signal, x^n. In GLM method, the original signal is supposed to be the activation coefficients multiplied by the design matrix. Since it is here tried to denoise the signal, therefore, the design matrix has been replaced and developed using impulses train (stimuli vector) to better apply the deconvolution algorithm. In general GLM formulation, the convolution operation appears in the matrix form (design matrix). Then, the GLM model is also here used but in the vectorial form not in matrix format.

Given the orthonormal regression matrix W, the Discrete Wavelet Transform (DWT) of the noisy data is defined as:

$$c^n = W^T y^n \quad (2)$$

Table 1. Percent of voxels change.

Subjects group	region-of-interests (ROIs)	
	Vision	motor
Elderly subjects	60.66 %	59.22 %
Young subjects	62.52 %	67.57 %

NEUROSCIENCE

Minimum Description Length (MDL) principle may be used to classify the coefficients into two categories: signal and noise. The MDL classification tries to achieve the minimum description of both data and the model itself simultaneously (Grünwald, 2007; Grünwald, Myung, & Pitt, 2005; Rissanen, 1996; Rissanen, 1978). The length of the description is defined by the negative logarithm of the so-called Normalized Maximum-Likelihood (NML) expression (Roos, Myllymaki, & Rissanen, 2009; Rissanen, 2000). The NML represents a universal model supposing a parametric distribution profile with parameters $\hat{\theta}(y^n)$ as following (Hirai, & Yamanishi, 2011; Meena, & Annadurai; 2008; Rissanen, 2001):

$$f_{nml}(y^n) = \frac{f(y^n; \hat{\theta}(y^n))}{\int_A f(z^n; \hat{\theta}(y^n)) dz^n} \quad (3)$$

Where A stands for the set of coefficients with length n. $\hat{\theta}(y^n)$ is the maximum likelihood estimate of the parameters. The NML is used to evaluate the complexity of different model classes in order to select the one associated with the minimum cost.

In MDL-based denoising, k coefficients are retained and the remaining n-k are considered as pure noise and set to zero. In crude MDL (C-MDL), a subset γ including

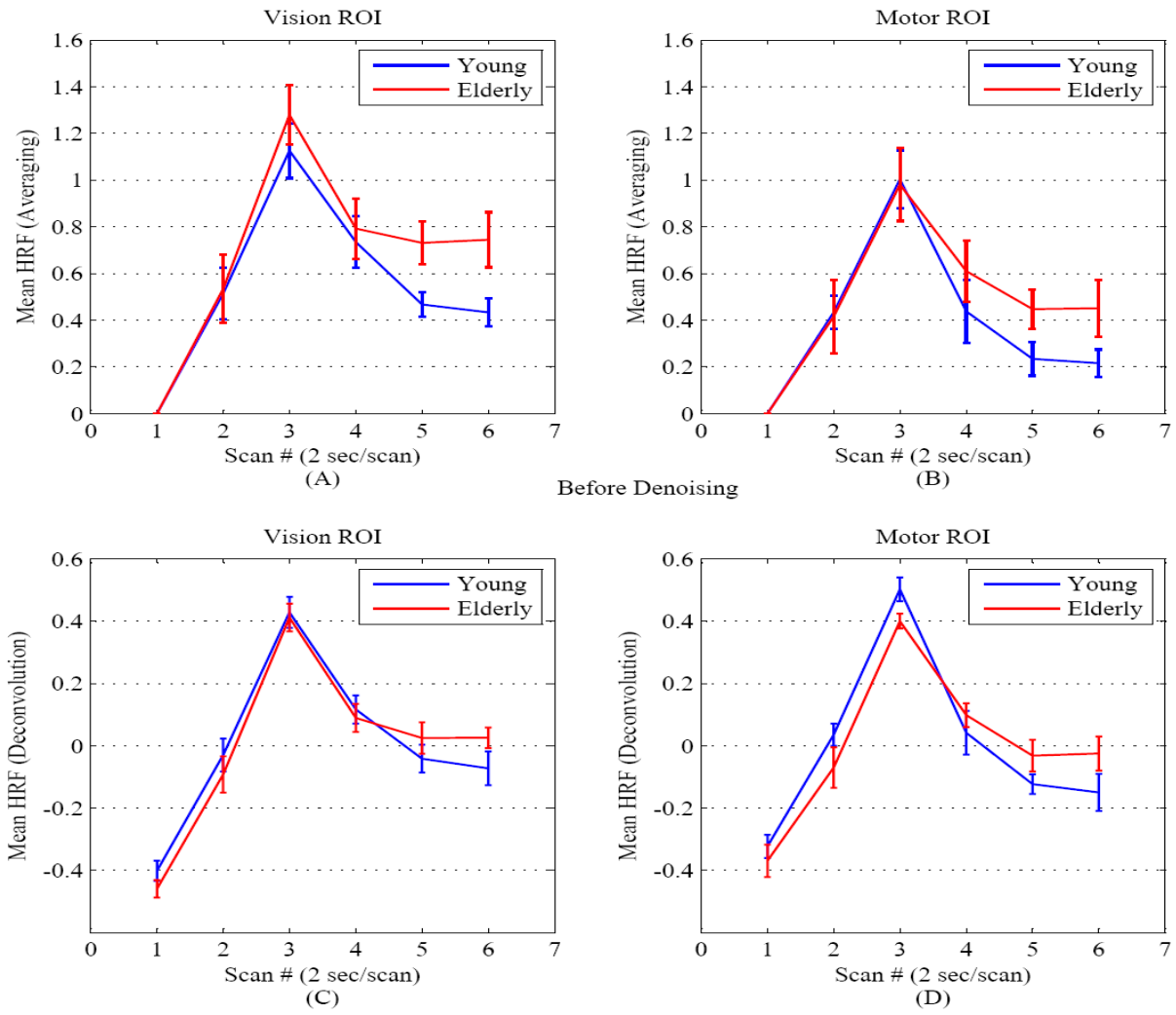

NEUROSCIENCE

Figure 5. Mean HRF using Averaging (A-B) and Deconvoultion (C-D) methods without denoising process for the young (blue) and old (red) subjects. Avergaing: (A) vision ROI (Aizenstein et al., 2004), (B) motor ROI (Aizenstein et al., 2004), and Deconvolution: (C) vision ROI and (D) motor ROI. Error bars represent ± 1 SEM.

k wavelet coefficients with largest absolute values are selected to minimize the following cost function (Rissanen, 2000):

$$\frac{n-k}{2}\ln\frac{S\left(y^{n}\right)-S_{\gamma}\left(y^{n}\right)}{n-k}+\frac{k}{2}\ln\frac{S_{\gamma}\left(y^{n}\right)}{k}+\frac{1}{2}\ln k\left(n-k\right) \quad (4)$$

Here, S (y^n) and S_γ (y^n) denote the sum squares of all wavelet coefficients and the coefficients belonging to γ respectively. The number of coefficients in γ is equal to k and n is the length of time series. The upper limit for k is held as k<0.95n (Roos, Myllymaki & Rissanen, 2009).

In refined MDL (R-MDL) as discussed in (Roos, Myllymaki, & Rissanen, 2009) the criterion has been changed to:

$$\frac{n-k}{2}\ln\frac{S\left(y^{n}\right)-S_{\gamma}\left(y^{n}\right)}{\left(n-k\right)^{3}}+\frac{k}{2}\ln\frac{S_{\gamma}\left(y^{n}\right)}{k^{3}} \quad (5)$$

Equation (4) is substituted by (5) as there are not so many classes in most cases. In the cases where the number of model classes is large, the selection of class index is vital. In the case of denoising, the number of different model classes increases up to 2n. Then, the encoding of the class index is crucial for fMRI data denoising (Roos, Myllymaki & Rissanen, 2009).

3. Results

3.1. Denoising Effects on Activation Detection

The effects of denoising fMRI data are here studied on the selection of activated voxels. The noise contribution gets larger and more important through age increasing (D'Esposito, Deouell, & Gazzaley, 2003; Huettel et al., 2001; & D'Esposito et al., 1999). The anatomically-identified ROIs for each subject were used to generate all time series associated with each trial in both the vision and motor regions. For both the vision and motor regions, all time series were firstly denoised by R-MDL for both the young and the elderly subjects (Morsheddost et al., 2014) followed by the t-test for selecting activated voxels. The activated voxels have been selected as shown in Figure 3 (vision) and Figure 4 (motor).

In both vision and motor regions, the initial connected regions of activated voxels (before denoising) have been extended either in the elderly or the young cases after denoising. In the elderly adults, new connected sub regions or spots have been nonetheless, appeared as well. It may be referred to the lower SNR of fMRI data in the elderly (0.35) compared to the young (0.52) (D'Esposito et al., 2003; Huettel et al., (2001)). The correlation of fMRI data of different voxels may decrease because of independent noise elements. Hence, denoising leads to an extension of activated voxels sub regions. In the elderly, the large contribution of noise may have yield the disappearance of activated spots or little sub regions.

Table 2. Finding on the comparison of HRF peak amplitudes between the elderly and the young adults.

Study Reference	region-of-interests (ROIs)	
	Vision	motor
This work (2014)	[E] = [Y]	[E] < [Y]
Mohtasib et al., (2012)	-	[E] > [Y]
Aizenstein et al., (2004)	[E] = [Y]	[E] = [Y]
Huettel et al., (2001)	[E] = [Y]	[E] = [Y]
Buckner et al., (2000)	[E] < [Y]	[E] = [Y]
D'Esposito et al., (1999)	-	[E] = [Y]
Ross et al., (1997)	[E] < [Y]	-
Gauthier et al., (2013)	Grey matter of the whole brain	
	[E] < [Y]	

[E]: HRF amplitude peak of elderly adults.
[Y]: HRF amplitude peak of young adults.

To better evaluate the denoising process, the activated voxels of the Top32 correlation are compared before and after denoising. Table 1 demonstrates the percent of activated voxels of Top32 correlation being not common before and after denoising. Accordingly, the noise appears to be dominant in the activation detection.

3.2. Mean HRF Extraction

3.2.1. Before denoising

The data reported in this experiment have been downloaded from the fMRI Data Center (http://www.fmridc.org) with accession number 2-2003-114FB. All qualifications (as paradigm and image acquisition) for all participants are equal. The identified ROIs for each subject were used to generate a mean HRF associated with each trial in both the vision and motor regions. The voxels with negative t-values were not included in the generation of the mean HRF. The HRF from the positive t-values extracted by averaging are shown in Figure 5 (A, & B) (Aizenstein et al., 2004). Results for both regions are same as Aizenstein et al., (2004) because data and method of extracting are same (before denoising). For both the vision (P=0.39) and motor (P=0.91) regions, the HRF amplitude peaks were similar for both the young and the elderly subjects by averaging. In the proposed work like Aizenstein et al., (2004), the fMRI data bank used includes only 6 scans at each BOLD time series associated with each stimulus. 6 time points are so few for fitting HRF conventional (Gamma etc) models to extract timing information. In addition, all previous papers (Gauthier et al., 2013; Mohtasib et al., 2012; Aizenstein et al., 2004; Huettel, Singerman, & McCarthy, 2001; Buckner, Snyder, Sanders, Raichle, & Morris, 2000; D'Esposito, Zarahn, Aguirre, & Rypma, 1999; Ross et al., 1997) studied in this work, changes in amplitude have examined. Also Modulation of the amplitude of the HRF arising from a brief, temporally well-characterized stimulus would be consistent with neuronal mechanisms, e.g. altered firing rates and synaptic input (Muthukumaraswamy, Evans, Edden, Wise, & Singh, 2012). As expected, the HRF peaked between 4 and 6 sec. There was, nonetheless, a significant difference between the groups in the degree of sustained activation. The HRF of elderly adults was significantly larger than the young subjects' HRF at scan 6 (10–12 sec) in the vision region (P<0.03) according to two-tailed test, and there was a trend for this difference in the motor region (P=0.11) at scan 6, two tailed test. The difference in the degree of sustained activation is consistent with the time series as Buckner et al., (2000) presents, but contrasts with the results of Huettel et al., (2001) and D'Esposito et al., (1999).

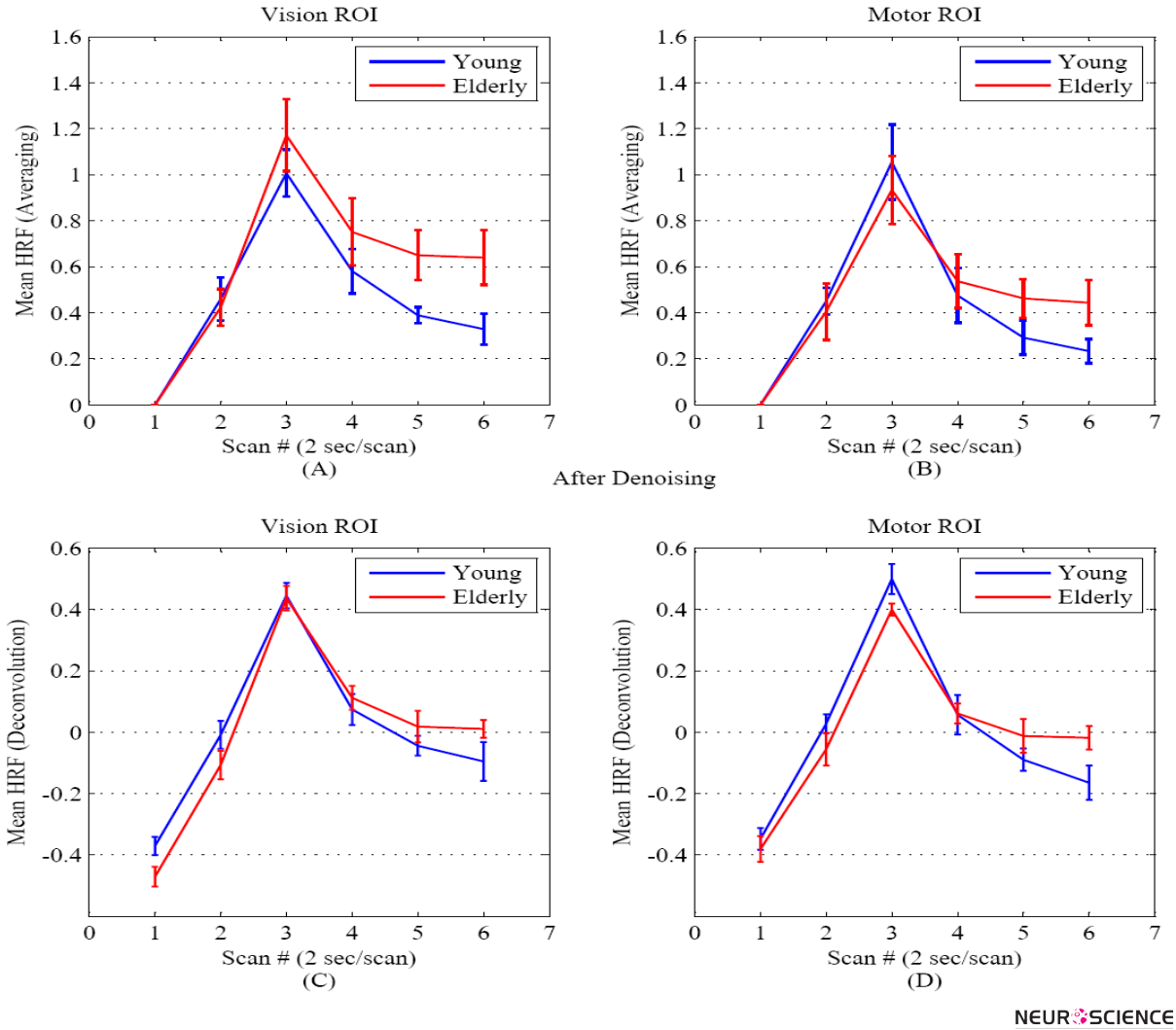

Figure 6. Mean HRF using Averaging (A-B) and Deconvoultion (C-D) methods applied after denoising process for the young (blue) and old (red) subjects. Avergaing: (A) vision ROI, (B) motor ROI, and Deconvolution: (C) vision ROI and (D) motor ROI. Error bars represent ± 1 SEM.

Figure 5 (C, & D) illustrates mean HRF extracted by deconvolution for each subject at both ROIs. In vision region, the HRF amplitude peaks were similar (P=0.80) and at scan 6 (10–12 sec) the HRF of elderly subjects is not significantly higher than the young subjects' HRF (P=0.13). But in motor ROI, the HRF amplitude peaks of young subjects were significantly higher than the HRF amplitude peaks of elderly subjects (P<0.03).

3.2.2. After denoising

The effects of fMRI data noise are here studied on the HRF estimation to compare the HRF extraction methods of averaging (used in earlier works) and deconvolution (this work).

Figure 6 demonstrates the HRF extracted after denoising fMRI data for visual and motor cortices. Figures 6-(A-B) and 6-(C-D) are associated with the averaging and the deconvolution techniques respectively. In the case of averaging algorithm, no significant difference, between the elderly and the young, is observed at the peak amplitude for vision (P=0.39) and motor (P=0.58) regions.

Figures 6-C and 6-D demonstrate the mean HRF extracted by deconvolution after denoising for vision and motor ROIs respectively. A significant difference is only obtained for motor region in which the young subjects exhibit a significant increase in the HRF amplitude peak compared with the elderly ones (P<0.06). The result of deconvolution after denoising is the same as found in the

earlier subsection for the case of fMRI data without denoising.

4. Discussion

In this study, a comparative study has been realized on the hemodynamic response properties associated with the young and the elderly adults on a simple visual and motor task. It was shown that the earlier works led to inconsistent findings on the HRF peak amplitudes because of averaging algorithm. In fact, fMRI data are heavily noisy particularly in the elderly case (e.g. D'Esposito et al., 2003; Huettel et al., 2001; D'Esposito et al., 1999). Accordingly, it is necessary to employ an HRF estimation algorithm which is sufficiently robust against noise. Averaging algorithm, used in all earlier similar works, cannot account for the noise challenge because of the related large sensitivity to outliers. The averaging sensitivity to noise worsens when the samples of the estimated function are few, like fMRI case (only 6 samples in this study). Employing the robust MDL-based wavelet denoising, it was shown that a large percent of the selected voxels changed in the activation detection at both motor and visual cortices (Figures 3 and 4). According to the experimentation results, the area of activated voxels is extended for both the elderly and the young. Though, the extension of activated voxels zone is larger for the elderly after denoising (Figures 3 and 4), but the amplitudes of time series appear to be more affected in the young case (Table 1).

In the step of HRF estimation, deconvolution appears to be much more robust against noise contribution because the related hemodynamic function is, at the same time, optimized through the whole time series scans. Consequently, the averaging method yields opposing results for HRF peak amplitudes as described in the earlier works (Table 2). However, deconvolution method has provided a robust HRF result. Considering deconvolution method, it may be concluded that the HRF peak amplitudes exhibit no significant difference in the visual cortex between the elderly and the young adults. Also, it can be deduced that the HRF peak amplitude of motor cortex is significantly larger for the young adults compared with the elderly ones.

The findings of current study have been summarized in the Table 2 in comparison with the earlier works. The divergence of earlier works on the results concerning HRF peak amplitude may be easily observed. Gauthier et al., have reported the HRF peak amplitude to be significantly larger for the young in comparison to the elderly through the cortex of the whole brain. Though, this work has predicted the same result for motor cortex, a hypothesis on HRF is better to be applied to limited functional zones in brain. More studies are required to be conducted for covering all functional regions on the brain cortex.

Acknowledgments

The data reported in this experiment have been downloaded from the fMRI Data Center (http://www.fmridc.org) with accession number 2-2003-114FB.

References

Aizenstein, H. J., Clark, K. A., Butters, M. A., Cochran, J., Stenger, V. A., Meltzer, C. C., Reynolds, C. F., & Carter C. S. (2004). The BOLD hemodynamic response in healthy aging. *Journal of Cognitive Neuroscience,* 16(5), 786-793.

Bandettini, P. A., Wong, E. C., Hinks, R. S., Tikofsky, R. S., & Hyde, J. S. (1992). Time course EPI of human brain function during task activation. *Magnetic Resonance in Medicine,* 25(2), 390-397.

Bazargani, N., Nosratinia, A. (2008). MDL-based Estimation of the Hemodynamic Response Function for fMRI data. *International Society of Magnetic Resonance in Medicine,* 16, 2479.

Boynton, G. M., Engel, S. A., Glover, G. H., & Heeger, D. J. (1996). Linear systems analysis of functional magnetic resonance imaging in human V1. *Journal of Neuroscience,* 16(3), 4207–4221.

Buckner, R. L., Snyder, A. Z., Sanders, A. L., Raichle, M. E., & Morris, J. C. (2000). Functional brain imaging of young, nondemented, and demented older adults. *Journal of Cognitive Neuroscience,* 12(Suppl 2), 24–34.

Cohen, J. D., MacWhinney, B., Flatt, M., & Provost, J. (1993). PsyScope: An interactive graphic system for designing and controlling experiments in the psychology laboratory using Macintosh computers. *Behavior Research Methods, Instruments, & Computers,* 25(2), 257–271.

D'Esposito, M., Deouell, L.Y., & Gazzaley, A. (2003). Alterations in the bold fMRI signal with ageing and disease: a challenge for neuroimaging. *Nature Reviews Neuroscience,* 4(11), 863-872.

D'Esposito, M., Zarahn, E., Aguirre, G. K., & Rypma, B. (1999). The effect of normal aging on the coupling of neural activity to the bold hemodynamic response. *Neuroimage,* 10(1), 6–14.

Donoho D. L., & Johnstone, I. M. (1995). Adapting to unknown smoothness via wavelet shrinkage. *Journal of the American Statistical Association,* 90(432), 1200-1224.

Donoho D. L., & Johnstone, I. M. (1994). Ideal spatial adaptation via wavelet shrinkage. *Biometrika,* 81(3), 425–455.

Gauthier, C. J., Madjar, C., Desjardins-Crépeau, L., Bellec, P., Bherer, L., & Hoge R. D. (2013). Age dependence of hemodynamic response characteristics in human functional magnetic resonance imaging. *Neurobiology of Aging,* 34(5), 1469-1485.

Grünwald, P. D. (2007). *The minimum description length principle.* Cambridge. MA: MIT Press.

Grünwald, P. D., Myung, I. J., & Pitt, M. A. (2005). *Advances in Minimum Description Length: Theory and Applications.* Cambridge, MA: MIT Press.

Hirai S., & Yamanishi, K. (2011). Efficient computation of normalized maximum likelihood coding for Gaussian mixtures with its applications to optimal clustering. *IEEE International Symposium on Information Theory Proceedings,* 1031–1035.

Huettel, S. A., Singerman, J. D., & McCarthy, G. (2001). The effects of aging upon the hemodynamic response measured by functional MRI. *Neuroimage,* 13(1), 161–175.

Jenkinson, M., Bannister, P., Brady, M., & Smith, S. (2002). Improved optimisation for the robust and accurate linear registration and motion correction of brain images. *Neuroimage,* 17(2), 825-841.

Jenkinson, M., & Smith, S. M. (2001). A global optimisation method for robust affine registration of brain images. *Medical Image Analysis,* 5(2), 143-156.

Mallat, S. (1998). *A wavelet tour of signal processing.* New York: Academic Press.

Meena, S., & Annadurai, S. (2008). Improved spatially adaptive MDL denoising of images using normalized maximum likelihood density. *Image & Vision Computing,* 26(11), 1524-1529.

Mohtasib, R. S., Lumley, G., Goodwin, J. A., Emsley, H. C., Sluming, V., & Parkes L. M. (2012). Calibrated fMRI during a cognitive stroop task reveals reduced metabolic response with increasing age. *Neuroimage,* 59(2), 1143-1151.

Morsheddost, H., Asemani D., & Mirahadi, N. (2014). Optimization of MDL-based wavelet denoising for fMRI data analysis. *IEEE International Symposium on Biomedical Imaging (ISBI),* 33-36.

Muthukumaraswamy, S. D., Evans, C. J., Edden, R. A. E., Wise, R. G., & Singh, K. D. (2012). Individual variability in the shape and amplitude of the BOLD-HRF correlates with endogenous GABAergic inhibition. *Human Brain Mapping,* 33(2), 455-465.

Ogawa, S., Menon, R. S., Tank, D. W., Kim, S. G., Merkle, H., Ellermann, J. M., & Ugurbil, K. (1993). Functional brain mapping by blood oxygenation level-dependent contrast magnetic resonance imaging. A comparison of signal characteristics with a biophysical model. *Biophysical Journal,* 64(3), 803-812.

Ogawa, S.,Tank, D. W., Menon, R., Ellermann, J. M., Kim, S. G., Merkle, H., & Ugurbil, K. (1992). Intrinsic signal changes accompanying sensory stimulation: functional brain mapping with magnetic resonance imaging. *Proceedings of the National Academy of Sciences,* 89(13), 5951-5955.

Ogawa, S., Lee, T. M., Kay, A. R., & Tank, D. W. (1990). Brain magnetic resonance imaging with contrast dependent on blood oxygenation. *Proceedings of the National Academy of Sciences, U.S.A.,* 87(24), 9868-9872.

Powers, R. (2000). *Neurobiology of aging.* In C. Coffey & J. Cummings (Eds.). The American Psychiatric Press testbook of geriatric neuropsychiatry (2nd ed.). Washington, DC: American Psychiatric Press.

Rissanen, J. (2001). Strong optimality of the normalized ML models as universal codes and information in data. *IEEE Transactions on Information Theory,* 47(5), 1712–1717.

Rissanen, J. (2000). MDL denoising. *IEEE Transactions on Information Theory,* 46(7), 2537–2543.

Rissanen, J. (1996). Fisher information and stochastic complexity. *IEEE Transactions on Information Theory,* 42(1), 40–47.

Rissanen, J. (1978). Modelling by shortest data description. *Automatica,* 14(5), 445–471.

Roos, T., Myllymaki, P., & Rissanen, J. (2009). MDL denoising revisited. *IEEE Transaction of Signal Processing,* 57(9), 839–849.

Ross, M. H., Yurgelun-Todd, D. A., Renshaw, P. F., Maas, L. C., Mendelson, J. H., Mello, N. K., Cohen, B. M., & Levin, J. M. (1997). Age-related reduction in functional MRI response to photic stimulation. *Neurology,* 48(1), 173–176.

Smith, S. (2002). Fast Robust Automated Brain Extraction. *Human Brain Mapping,* 17(3), 143-155.

Tzourio-Mazoyer, N., Landeau, B., Papathanassiou, D., Crivello, F., Etard, O., Delcroix, N., Mazoyer, B., & Joliot, M. (2002). Automated anatomical labelling of activations in SPM using a macroscopic anatomical parcellation of the MNI MRI single-subject brain. *Neuroimage,* 15(1), 273–289.